ROYAL SOCIETY
OF CHEMISTRY

PAPER

Check for updates

A multimodal caffeic acid-derived alkyl-amide antidiabetic agent: targeting α-glucosidase, α-amylase, oxidative stress, and protein glycation

Karthika Kannan [a] and Sushabhan Sadhukhan *[ab]

Historically, natural products have been a primary source of new drugs and lead compounds. However, their direct application as therapeutic agents remains limited. Given the multifactorial nature of diabetes, therapeutic agents with multi-targeting properties offer a promising solution for effective management. Herein, we developed a library of seven lipophilic derivatives of caffeic acid (CA) and evaluated their multimodal antidiabetic activities. Among these, the most potent compound, **CA14**, showed an IC_{50} of 1.94 μM, representing a 113-fold improvement over acarbose (IC_{50} 219.70 μM). Further, compared to the parent compound CA (IC_{50} 12 400 μM), **CA14** was 6392 times more potent. Kinetic analysis revealed that **CA14** acts as a competitive inhibitor of α-glucosidase. **CA14** showed comparable α-amylase inhibition to that of acarbose, while CA showed no inhibition even at 500 μM. Additionally, **CA14** exhibited antiglycation activity by inhibiting fructosamine and advanced glycation end products (AGEs). It also showed excellent antioxidant activity (IC_{50} 13.98 μM), nearly twice as potent as Vitamin C. Notably, acarbose lacked any antioxidant activity. Intrinsic fluorescence quenching and FT-IR analyses further confirmed that **CA14** disrupted substrate binding, reducing enzymatic activity. Of note, **CA14** did not exhibit any significant cytotoxicity in 3T3-L1 fibroblasts, even at 50 μM. Molecular docking revealed good extent of interactions, while ADMET profiling predicted favorable druglikeness. **CA14** was found to be stable under physiological conditions even after 10 days. In summary, CA derivatives demonstrated robust multifaceted antidiabetic potential by inhibiting α-glucosidase, α-amylase, and AGE formation, while also mitigating oxidative stress, which are key contributors to diabetes progression.

1. Introduction

Diabetes mellitus manifests as a pathological dysregulation of postprandial glucose homeostasis, leading to aberrant carbohydrate metabolism and a cascade of systemic pathophysiological consequences. Starch, contributing about 50–70% of energy, is hydrolyzed by α-amylase to reducing sugars. These are then converted to glucose by α-glucosidase present at the brush border of small intestine.[1,2] Hyperglycemia may stem from either type 1 diabetes mellitus (T1DM), which is characterized by a lack of insulin secretion, or type 2 diabetes mellitus (T2DM), which is characterized by cellular resistance towards insulin.[3–5] The International Diabetes Federation (IDF) projects that by 2050, 852.5 million people will be diabetic.[6] Diabetes ranks ninth among the world's leading causes of mortality, affecting one in ten persons worldwide making it an unprecedented pandemic over time.[7]

Hyperglycemia often elevate the reactive oxygen species (ROS), thereby creating an environment that predisposes cells to insulin resistance[8] and accelerate the non-enzymatic glycation of proteins, giving rise to advanced glycation end products (AGEs).[9,10] Currently, the primary therapeutic strategy for managing hyperglycemia involves inhibiting α-amylase and α-glucosidase, thereby delaying carbohydrate hydrolysis.[11,12] To date, acarbose and miglitol are the food and drug administration (FDA)-approved drugs, which target these enzymes[12,13] but its extended use has resulted in several side effects including, liver problems, abdomen discomfort, vomiting.[14,15] Furthermore, the drugs with a strong α-amylase inhibition are found to result in severe gastrointestinal problems.[16–18] Aminoguanidine (AG), a potent inhibitor of non-enzymatic glycation,[19] has been associated with significant toxicity concerns, as identified during clinical trials.[20] AGEs, ROS, smoking, obesity and diabetes mutually exacerbate each other, making it complicated.[21–23]

Nature is a bedrock of drug discovery, which inspires scientists to look back for the development of effective therapeutics.[24,25] Polyphenols are one of the naturally occurring compounds having wide range of pharmaceutical effects without any significant cytotoxicity.[26,27] Caffeic acid (CA),

[a]Department of Chemistry, Indian Institute of Technology Palakkad, Palakkad, Kerala 678 623, India. E-mail: sushabhan@iitpkd.ac.in

[b]Physical & Chemical Biology Laboratory and Department of Biological Sciences & Engineering, Indian Institute of Technology Palakkad, Palakkad, Kerala 678 623, India

a naturally occurring hydroxycinnamic acid, is a category of phenolic acid that is widely distributed in various plant-based foods, including coffee, fruits, vegetables, and herbs.[28,29] Its diverse pharmacological properties make it a promising compound for the development of novel therapeutic agents.[26,30,31]

Our group has recently reported epigallocatechin-3-gallate (EGCG)-quinoxaline hybrids obtained through the click reaction as potent α-amylase and α-glucosidase inhibitors along with strong antioxidant activity.[32] Furthermore, we have also reported lipophilic derivatives of EGCG, having strong antidiabetic, antioxidant, as well as anti-inflammatory properties.[33] A similar trend was demonstrated by Wang *et al.* showing an increasing trend of α-amylase and α-glucosidase inhibitory activity with an increase in the hydrophobic chain on chlorogenic acid.[34] High glucose level and oxidative stress often leads to the accumulation of excess cholesterol in the cellular membrane, which in turn triggers several other complications.[35] Interestingly, a report by Sherratt *et al.* demonstrated that lipophilic ester derivatives of rosmarinic acid can inhibit the formation of cholesterol domains in model membranes through their antioxidant properties.[36] The carbohydrate hydrolase inhibitory effects of EGCG palmitate by Liu *et al.* further underscore an enhanced antidiabetic activity achieved through lipophilization.[37] However, the high molecular weight may pose challenges to its bioavailability.

Given that diabetes is a multifactorial problem, unlike the "one drug-one target approach", it requires a multi-targeting approach to effectively tackle the disease.[38,39] In this connection, we aimed to develop lipophilic derivatives of low molecular weight CA, and generated a library of CA*n*, where *n* represents even numbers ranging from 4 to 16, to evaluate it as a multi-targeting antidiabetic agent. Among the synthesized derivatives, **CA14** emerged as the most potent, demonstrating significant inhibition of α-glucosidase and α-amylase, along with strong antioxidant and antiglycation activities. The interaction of **CA14** with the target proteins was further validated using Fourier transform-infrared spectroscopy (FT-IR). Microenvironmental changes and the resulting intrinsic fluorescence quenching behaviour of the enzymes upon interaction with **CA14** was investigated. Molecular docking was employed to gain insights into the interactions between key amino acids and the potent compound. *In silico* absorption, distribution, metabolism, excretion, and toxicity (ADMET) profiling of **CA14** was studied to predict the druglikeness and pharmacokinetic properties. Further, **CA14** was found to be stable under physiological conditions. Moreover, **CA14** exhibited no significant cytotoxicity even at concentrations up to 50 μM in 3T3-L1 cells. These findings reinforce the potential of nature as a vast reservoir of bioactive molecules, offering promising avenues for the development of effective multimodal antidiabetic therapeutics.

2. Experimental section

2.1 Materials used

Caffeic acid (CA), Girard's T reagent, tetradecylamine, and aminoguanidine hydrochloride were procured from BLD

Pharmatech Co. Ltd, India. Acarbose, α-glucosidase (Cat. No. G5003), porcine pancreatic α-amylase (Cat. No. A3176), 3,5-dinitrosalicylic acid (DNS) and potato starch were purchased from Sigma-Aldrich, USA. 3-(4,5-Dimethylthiazol-2-yl)-2,5-diphenyltetrazolium bromide (MTT), fructose, *p*-nitrophenyl-α-D-glucopyranoside (α-pNPG), nitroblue tetrazolium (NBT), bovine serum albumin (BSA), *N*,*N*′-dicyclohexylcarbodiimide (DCC), dodecylamine, butylamine, hexadecylamine, and L-ascorbic acid were procured from the Sisco Research Laboratories (SRL) Pvt. Ltd, India. Decylamine was procured from Chemscene Jinay Pharmaceuticals Pvt. Ltd, India. Silica gel 60–120, *n*-hexylamine, *n*-octylamine, and *n*-octadecylamine were purchased from Spectrochem, India. Reagent-grade solvents were procured from Pure Chem Pvt. Ltd, India.

2.2 Instruments and methods used

Shimadzu liquid chromatography-mass spectrometry (LC-MS)-8045 with a Sprite TARGA C18 column (40 × 2.1 mm, 5 μm) was used for LC-MS analysis. Water with 0.1% formic acid was used as solvent A for the HPLC, while acetonitrile with 0.1% formic acid was used as solvent B. At a flow rate of 0.5 mL min⁻¹, compounds were eluted using a gradient of 5% solvent B for 1 minute, a linear gradient of 5% to 60% solvent B over 5 minutes, continued for 1 minute, a gradient of 60% to 95% solvent B in 3 minutes, continued for another 3 minutes, and then a gradient of 5% solvent B in 1.5 minutes, brought down to 5% solvent B in 1.5 minutes and then continued for another 1.5 minutes before the method was stopped. Before injecting the sample, the column was always rinsed with 50% solvent B and then 95% solvent B. ^{1}H and ^{13}C NMR spectra were recorded in the AVANCE NEO500 Ascend Bruker BioSpin International AG NMR spectrometer. ^{1}H and ^{13}C NMR spectra were recorded in DMSO-d_6, and the spectral data were reported in ppm. The absorbance values for all the assays were measured using microplate reader (BioTek, Epoch 2). FT-IR spectra were recorded using a PerkinElmer Spectrum 100 spectrometer using universal attenuated total reflectance (ATR).

2.3 General procedure for the synthesis of CA alkyl-amide derivatives (CA*n*)

The lipophilic CA derivatives were synthesized according to the previously reported protocol with slight modifications.[40] In brief, DCC (228 mg, 1.11 mmol, 1 eq.) was introduced into a well-stirred solution of CA (200 mg, 1.11 mmol, 1 eq.) in 10 mL of dry tetrahydrofuran (THF). The mixture was allowed to stir for about 5 minutes followed by the dropwise addition of alkan-1-amine (1.11 mmol, 1 eq.). The solution was stirred at 60 °C and the reaction progress was monitored using the thin-layer chromatography (TLC). The reaction was quenched after 4 hours with 5 mL of water and extracted with ethyl acetate (5 mL × 3), followed by the addition of anhydrous sodium sulphate to remove residual water from the organic layer. The organic solvent was evaporated under reduced pressure and purified using silica gel column chromatography (acetone/dichloromethane). The compounds were characterized using LC-MS, ^{1}H NMR, and ^{13}C NMR (Fig. S1–S28).

2.3.1 (E)-3-(3,4-Dihydroxyphenyl)-N-butylacrylamide (CA4). Yield: 70%. MS (ESI): m/z calculated for $[C_{13}H_{17}NO_3 + H]^+ = 236.12$, observed is 236.30. ^1H NMR (500 MHz, DMSO-d_6): δ (ppm) = 0.88 (3H, t, J = 7.00 Hz), 1.30 (2H, sext, J = 7.00 Hz), 1.42 (2H, quint, J = 7.00 Hz), 3.14 (2H, q, J = 6.50 Hz), 6.32 (1H, d, J = 15.50 Hz), 6.74 (1H, d, J = 8.00 Hz), 6.82 (1H, dd, J = 8.00, 2.00 Hz), 6.93 (1H, d, J = 2.00 Hz), 7.21 (1H, d, J = 15.50 Hz), 7.94 (1H, t, J = 6.00 Hz). ^{13}C NMR (125 MHz, DMSO-d_6): δ (ppm) = 13.73, 19.68, 31.37, 38.32, 113.83, 115.77, 118.68, 120.36, 126.48, 138.90, 145.55, 147.25, 165.33.

2.3.2 (E)-3-(3,4-Dihydroxyphenyl)-N-hexylacrylamide (CA6). Yield: 75%. MS (ESI): m/z calculated for $[C_{15}H_{21}NO_3 + H]^+ = 264.15$, observed is 264.30. ^1H NMR (500 MHz, DMSO-d_6): δ (ppm) = 0.86 (3H, t, J = 7.00 Hz), 1.26 (6H, bs), 1.43 (2H, quin, J = 7.00 Hz), 3.13 (2H, q, J = 6.50 Hz), 6.31 (1H, d, J = 15.50 Hz), 6.73 (1H, d, J = 8.00 Hz), 6.82 (1H, dd, J = 8.00, 2.00 Hz), 6.93 (1H, d, J = 2.00 Hz), 7.20 (1H, d, J = 15.50 Hz), 7.94 (1H, t, J = 6.00 Hz). ^{13}C NMR (125 MHz, DMSO-d_6): δ (ppm) = 13.96, 22.09, 26.20, 29.22, 31.04, 38.64, 113.81, 115.75, 118.67, 120.33, 126.46, 138.86, 145.53, 147.22, 165.27.

2.3.3 (E)-3-(3,4-Dihydroxyphenyl)-N-octylacrylamide (CA8). Yield: 68%. MS (ESI): m/z calculated for $[C_{17}H_{25}NO_3 + H]^+ = 292.18$, observed is 292.30. ^1H NMR (500 MHz, DMSO-d_6): δ (ppm) = 0.86 (3H, t, J = 7.00 Hz), 1.26 (10H, bs), 1.43 (2H, quin, J = 7.00 Hz), 3.13 (2H, q, J = 6.50 Hz), 6.31 (1H, d, J = 15.50 Hz), 6.73 (1H, d, J = 8.00 Hz), 6.82 (1H, dd, J = 8.00, 2.00 Hz), 6.93 (1H, d, J = 2.00 Hz), 7.20 (1H, d, J = 15.50 Hz), 7.93 (1H, t, J = 6.00 Hz). ^{13}C NMR (125 MHz, DMSO-d_6): δ (ppm) = 13.99, 22.12, 26.53, 28.69, 28.77, 29.24, 31.28, 38.63, 113.81, 115.75, 118.68, 120.33, 126.46, 138.86, 145.53, 147.23, 165.27.

2.3.4 (E)-3-(3,4-Dihydroxyphenyl)-N-decylacrylamide (CA10). Yield: 76%. MS (ESI): m/z calculated for $[C_{19}H_{29}NO_3 + H]^+ = 320.21$, observed is 320.40. ^1H NMR (500 MHz, DMSO-d_6): δ (ppm) = 0.85 (3H, t, J = 7.00 Hz), 1.24 (16H, bs), 1.43 (2H, bs), 3.13 (2H, q, J = 6.50 Hz), 6.31 (1H, d, J = 15.50 Hz), 6.73 (1H, d, J = 8.00 Hz), 6.82 (1H, dd, J = 8.00, 2.00 Hz), 6.93 (1H, d, J = 2.00 Hz), 7.21 (1H, d, J = 15.50 Hz), 7.93 (1H, t, J = 6.00 Hz). ^{13}C NMR (125 MHz, DMSO-d_6): δ (ppm) = 13.97, 22.13, 26.52, 28.74, 28.81, 29.00, 29.05, 29.25, 31.33, 38.63, 113.81, 115.74, 118.68, 120.31, 126.48, 138.86, 145.55, 147.23, 165.28.

2.3.5 (E)-3-(3,4-Dihydroxyphenyl)-N-dodecylacrylamide (CA12). Yield: 72%. MS (ESI): m/z calculated for $[C_{21}H_{33}NO_3 + H]^+ = 348.25$, observed is 348.45. ^1H NMR (500 MHz, DMSO-d_6): δ (ppm) = 0.85 (3H, t, J = 7.00 Hz), 1.24 (18H, bs), 1.42 (2H, bs), 3.13 (2H, q, J = 6.50 Hz), 6.31 (1H, d, J = 15.50 Hz), 6.73 (1H, d, J = 8.00 Hz), 6.82 (1H, d, J = 8 Hz), 6.93 (1H, bs), 7.21 (1H, d, J = 15.50 Hz), 7.93 (1H, t, J = 6.00 Hz). ^{13}C NMR (125 MHz, DMSO-d_6): δ (ppm) = 13.98, 22.13, 26.51, 28.74, 28.79, 29.03, 29.04, 29.08, 29.23, 31.33, 38.63, 113.81, 115.74, 118.67, 120.31, 126.46, 138.85, 145.53, 147.22, 165.27.

2.3.6 (E)-3-(3,4-Dihydroxyphenyl)-N-tetradecylacrylamide (CA14). Yield: 76%. MS (ESI): m/z calculated for $[C_{23}H_{37}NO_3 + H]^+ = 376.28$, observed is 376.50. ^1H NMR (500 MHz, DMSO-d_6): δ (ppm) = 0.84 (3H, t, J = 7.00 Hz), 1.23 (22H, bs), 1.42 (2H, bs), 3.13 (2H, q, J = 6.50 Hz), 6.31 (1H, d, J = 15.50 Hz), 6.73 (1H, d, J = 8.00 Hz), 6.82 (1H, dd, J = 8.00, 2.00 Hz), 6.93 (1H, d, J = 2.00 Hz), 7.21 (1H, d, J = 15.50 Hz), 7.93 (1H, t, J = 6.00 Hz). ^{13}C NMR (125 MHz, DMSO-d_6): δ (ppm) = 13.98, 22.13, 26.52, 28.75, 28.81, 29.04, 29.05, 29.08, 29.09, 29.24, 31.33, 38.63, 113.81, 115.74, 118.66, 120.30, 126.47, 138.86, 145.53, 147.22, 165.27.

2.3.7 (E)-3-(3,4-Dihydroxyphenyl)-N-hexadecylacrylamide (CA16). Yield: 73%. MS (ESI): m/z calculated for $[C_{25}H_{41}NO_3 + H]^+ = 404.31$, observed is 404.50. ^1H NMR (500 MHz, DMSO-d_6): δ (ppm) = 0.85 (3H, t, J = 7.00 Hz), 1.23 (26H, bs), 1.42 (2H, bs), 3.13 (2H, q, J = 6.50 Hz), 6.31 (1H, d, J = 15.50 Hz), 6.73 (1H, d, J = 8.00 Hz), 6.82 (1H, dd, J = 8.00, 2.00 Hz), 6.92 (1H, d, J = 2.00 Hz), 7.20 (1H, d, J = 15.50 Hz), 7.93 (1H, t, J = 6.00 Hz). ^{13}C NMR (125 MHz, DMSO-d_6): δ (ppm) = 13.99, 22.13, 26.51, 28.74, 28.80, 29.03, 29.07, 29.24, 31.33, 38.63, 113.82, 115.75, 118.67, 120.32, 126.47, 138.87, 145.54, 147.22, 165.28.

2.4 α-Glucosidase inhibitory activity of CAn derivatives

All the synthesized derivatives were examined for their inhibitory potential using the previously reported protocol by our group.[32] In brief, α-glucosidase solution (0.3 U mL^{-1}) was prepared in a 50 mM sodium phosphate buffer of pH 6.8. The test samples (standard or CA derivatives) were dissolved in 20% DMSO in buffer to study the inhibition. 80 µL of different inhibitor concentrations were mixed with 20 µL of the enzyme solution and incubated for 10 minutes at 37 °C. Of note, mixture of 80 µL of 20% DMSO in buffer solution and 20 µL enzyme solution served as the control. After preincubation, 100 µL of 200 µM pNPG as a substrate was added to the enzyme and inhibitor solution, followed by an incubation for 30 minutes. The reaction was quenched by adding 80 µL of 200 mM sodium carbonate solution followed by an absorbance reading at 405 nm using microplate reader. The following equation was used to assess the α-glucosidase inhibitory activity, where Abs$_c$ represents the absorbance of the control, and Abs$_s$ represents the absorbance of the sample. The IC$_{50}$ values were calculated from the non-linear regression curves using GraphPad Prism 8 (GraphPad Software Inc., USA). The assay was performed in triplicate to ensure accuracy and reliability.

$$\alpha\text{-Glucosidase inhibition}(\%) = \left(\frac{\text{Abs}_c - \text{Abs}_s}{\text{Abs}_c}\right) \times 100$$

2.5 α-Amylase inhibitory activity of CAn derivatives

All the synthesized derivatives were examined for their inhibitory potential against α-amylase using the previously reported protocol by our group.[33] Briefly, an enzyme solution of 2 U mL^{-1} was prepared in 10 mM sodium phosphate buffer of pH 6.8 containing 0.5 mM NaCl. Test samples at varying concentrations were prepared in 20% DMSO in buffer. 100 µL of each inhibitor concentration and 100 µL of the enzyme were added to different micro-centrifuge tubes. The solution was preincubated at 37 °C for 10 minutes. For the control, inhibitor was replaced by 20% DMSO in the buffer. To all the tubes, 100 µL of 1% starch solution in buffer was added and incubated again for 10 minutes. The reaction was terminated by adding 200 µL of DNS was added in all tubes, followed by heating it in a dry bath at

100 °C for 5 minutes. For the absorbance reading at 540 nm, 50 μL of these solutions were taken in 96-well plate and diluted with 200 μL of distilled water. The percentage inhibitory activity was evaluated using the formula given below, where Abs_s and Abs_c hold the standard meaning. IC_{50} values were determined using non-linear regression analysis in GraphPad Prism 8 (GraphPad Software Inc., USA). The assay was performed in triplicate to ensure accuracy and reliability.

$$\alpha\text{-Amylase inhibition}(\%) = \left(\frac{Abs_c - Abs_s}{Abs_c}\right) \times 100$$

2.6 Free radical scavenging activity of CAn derivatives

The antioxidant capacity of the synthesized derivatives was determined using 2,2-diphenyl-1-picrylhydrazyl (DPPH) assay as per the previously reported protocol by our group using ascorbic acid as the control.[32] Briefly, 50 μL of different concentrations of the test compounds prepared in DMSO were added to 96-well plates. 150 μL of 0.2 mM DPPH in 95% methanol was added to each well and incubated for 1 hour in dark at room temperature followed by measuring the absorbance at 517 nm. The following formula was used to determine the free radical scavenging capacity where Abs_s and Abs_c hold the standard meaning. The IC_{50} values were calculated from the non-linear regression curves using GraphPad Prism 8 (GraphPad Software Inc., USA). The assay was performed in triplicate to ensure accuracy and reliability.

$$\text{Free radical scavenging activity}(\%) = \left(\frac{Abs_c - Abs_s}{Abs_c}\right) \times 100$$

2.7 Enzyme kinetics study

The mechanism of inhibition of the enzyme was determined using our reported protocol.[32,33] In brief, different concentrations (<IC_{50} value) of **CA14** and acarbose were mixed with 20 μL of 0.3 U per mL α-glucosidase and incubated at 37 °C for 10 minutes. Following preincubation, the solution was treated with α-pNPG (0.25–2 mM), followed by measuring the absorbance at 405 nm at 1 minute intervals for 30 minutes. Lineweaver–Burk plots ($1/V$ vs. $1/S$) were used to find the K_m and V_{max} values where S represents the concentration of the substrate, V denotes the rate of enzymatic reaction, K_m is the Michaelis–Menten, and V_{max} is the maximal reaction velocity. The K_i values were calculated using the competitive inhibition model in GraphPad Prism 8 (GraphPad Software Inc., USA).

2.8 Inhibitory study on non-enzymatic protein glycation

To evaluate the antiglycation potential of the most potent compound, we followed the protocol reported by Xu et al. employing the BSA-fructose model.[41,42] In brief, 300 mg of BSA and 900 mg of fructose were dissolved in 10 mL of 0.2 M potassium phosphate buffer of pH 7.4. 100 μL of BSA-fructose solution and 100 μL of varying concentrations of **CA14** were added in a 96 well plate, followed by incubation at 50 °C for

24 hours. The resulting mixture was then analysed for its inhibitory properties for the following. AG was used as a positive control for the AGEs inhibitory study. The experiments were performed in triplicate and used GraphPad Prism 8 (GraphPad Software Inc., USA) to determine the IC_{50}.

2.8.1 Study on fructosamine inhibition. The early formed non-enzymatic glycation product, fructosamine, was determined using NBT assay. To begin with, NBT (300 μM) was prepared in 0.1 M sodium carbonate buffer of pH 10.6. The incubated solution (10 μL) was treated with 100 μL of NBT solution and incubated at 37 °C for 15 minutes in a 96 well plate followed by measuring the absorbance at 530 nm. The following equation was used to measure the inhibition rate.

$$\% \text{ fructosamine inhibition} = \frac{(Abs_c - Abs_{cb}) - (Abs_s - Abs_{sb})}{(Abs_c - Abs_{cb})} \times 100$$

Abs_c and Abs_{cb} represent the absorbance of the control and control blank, respectively, whereas Abs_s and Abs_{sb} denote the absorbance of the sample and sample blank respectively.

2.8.2 Determination of the inhibitory action on AGEs. The fluorescence intensity of the incubated solution was recorded at an exciting wavelength of 375 nm and an emission wavelength of 440 nm. 20 μL of the incubation mixture was diluted to 100 μL in a 96 black well plate, followed by its fluorescence intensity measurement using a fluorescence spectrophotometer. The lower the intensity of fluorescence reflects less glycation end products. The inhibition rates by **CA14** and AG were calculated using the equation.

$$\% \text{ AGEs inhibition} = \frac{(I_c - I_{cb}) - (I_s - I_{sb})}{(I_c - I_{cb})} \times 100$$

I_c and I_{cb} represent the fluorescence intensity of the control and control blank, respectively, whereas I_s and I_{sb} denote the fluorescence intensity of the sample and sample blank, respectively.

2.9 Intrinsic fluorescence quenching and determination of binding affinity

We assessed the binding affinity of **CA14** towards both α-amylase and α-glucosidase using the methodology reported by our group.[32,33] In brief, the fluorescence spectra of both α-glucosidase (7 μM) and α-amylase (7 μM) solutions in the presence of varying concentrations of **CA14** (2–20 μM) were measured. The excitation wavelength was set at 280 nm, and fluorescence spectra were scanned from 300 to 500 nm. The slit width for excitation and emission was maintained at 10 nm for α-amylase and 5 nm for α-glucosidase. The maximal fluorescence intensity for α-amylase was observed at 348.4 nm and for α-glucosidase at 329.5 nm.

The extent of intrinsic fluorescence quenching by the compound (**CA14**) was measured by using the Stern–Volmer equation

$$\frac{I_0}{I} = 1 + K_{SV}[\mathbf{CA14}] = 1 + K_q \tau_0 [\mathbf{CA14}]$$

where I_0 is the intrinsic fluorescence of the enzymes without the inhibitor and I represent the fluorescence intensity of the enzyme upon addition of different concentrations of the inhibitor. K_{SV} and K_q were determined from the slope of the above equation whereas n and K_a was obtained from the Scatchard equation given below

$$\text{Log}((I_0/I) - 1) = \text{Log}\, K_a + n \log[\textbf{CA14}]$$

2.10 Docking studies with α-glucosidase and α-amylase

To begin with, we prepared the structure of acarbose and **CA14** in ChemBio3D Ultra 14.0 and minimized the energy and saved it as mol file. Using the Open Babel GUI tool we further converted the mol file to pdbqt format for docking. The molecular docking of **CA14** with α-glucosidase was performed in accordance with our previously reported protocol by our group.[33] In brief, we used SWISS-MODEL repository to obtain the structure of α-glucosidase MAL12 protein (P53341).[43] The protein was prepared by removing the water molecule, repairing missing atoms, adding polar hydrogens followed by Kollman charges, and a grid box dimension was set using AutoDock Vina (1.5.7) program.[44] The docking for **CA14** and acarbose was run using Perl script.[45] The protein–ligand interactions for the docked molecules were analysed using the BIOVIA Discovery Studio 2021.[46]

The molecular docking of **CA14** with α-amylase was performed in accordance with our previously reported protocol.[33] In brief, the structure of porcine pancreatic α-amylase with a PDB ID (1OSE) was retrieved from Protein Data Bank.[47] The protein was prepared by removing the water molecule, co-crystallized acarbose, repairing missing atoms, adding polar hydrogens, Kollman charges, and a grid box dimension was set using AutoDock Vina (1.5.7) program. The protein–ligand interactions for the docked molecules were analysed using the BIOVIA Discovery Studio 2021 while docking was carried out using Perl script.

2.11 FT-IR analysis

The non-covalent interactions between the enzyme and **CA14** were investigated using FT-IR spectrophotometer.[48] α-Glucosidase (7 μM) and α-amylase (7 μM) were prepared in 50 mM sodium phosphate buffer of pH 6.8, and % transmittance was recorded as the control. To assess the effect of **CA14**, a mixture of α-glucosidase and **CA14** (20 μM) was incubated at 37 °C for 30 minutes, while α-amylase was incubated with **CA14** (20 μM) at 37 °C for 10 minutes. Both samples were scanned across the spectral range (350–4500 cm^{-1}) at 0.2 cm^{-1} resolution.

2.12 Cytotoxicity studies in 3T3-L1 mammalian cell line

To check whether our potent compound is safe to use in mammalian cells, we performed an MTT assay based on the previously reported protocol by our group.[32,33] The 3T3-L1 cells were cultured in Dulbecco's modified eagle medium (DMEM) supplemented with 10% FBS, 1% penicillin–streptomycin, and 0.2% amphotericin, and maintained at 37 °C in a humidified

5% CO_2 incubator. In a 96-well plate, 2.0×10^4 cells per well were seeded and incubated overnight in DMEM. Adhered cells were washed with 1X phosphate-buffered saline (PBS), and then treated with different concentrations of **CA14** (0–50 μM) prepared in DMEM for 12 hours. After incubation, each well was washed with 1X PBS and treated with 0.05% MTT solution in DMEM followed by 3 hours incubation. The media was aspirated out and the resultant formazan crystals were dissolved in 100 μL DMSO. The absorbance of the resultant violet solution was measured at 590 nm with a reference wavelength assessed at 620 nm. A non-linear regression analysis was performed to assess the IC_{50} using the GraphPad Prism 8 (GraphPad Software Inc., USA). The assay was performed in triplicate to ensure the accuracy and reliability.

2.13 *In silico* evaluation of druglikeness and pharmacokinetic characteristics

To check the physicochemical properties of **CA14**, we utilized SwissADME analysis,[49] which includes the parameters such as molar mass, lipophilicity, number of hydrogen bond donors and acceptors, topological polar surface area (TPSA), and number of rotatable bonds. Additionally, we employed ADMET profiling to predict the absorption, distribution, metabolism, excretion, and toxicity of the designed molecule using the pkCSM web tool.[50] These findings help in assessing whether the molecule can advance its therapeutic potential as a drug.[51]

2.14 Stability assay of CA14 under physiological conditions

The stability of the lead compound, **CA14**, was studied under the physiological conditions (1X PBS pH 7.4 and 37 °C) with the help LC-MS using the previously reported method.[33] Briefly, a 200 μM solution of **CA14** was prepared in 1X PBS of pH 7.4 and incubated at 37 °C. Immediately after preparation, 500 μL of the solution was collected separately in a vial and extracted with ethyl acetate (100 μL × 3). The organic layer was evaporated under reduced pressure and stored at −20 °C to determine the stability of the compound at 0$^{\text{th}}$ hour. After 10 days of incubation, the sample was further extracted with ethyl acetate and the residue was collected upon evaporation. The stability of **CA14**, thus collected at 0$^{\text{th}}$ hour and 10$^{\text{th}}$ day, was analysed *via* LC-MS.

2.15 Statistical analysis of the data

We used GraphPad Prism 8 software to perform the statistical analysis. One-way analysis of variance (ANOVA), with Dunnett's multiple comparison test and Student's t-test, was used to determine the statistical significance of the data, where 'ns' represents not significant and is given for $p > 0.05$, * for $p < 0.05$, and ** for $p < 0.01$. All the data in this manuscript, including the IC_{50} values, are represented as mean ± standard error of the mean (SEM) from the experiments conducted in triplicate.

3. Results and discussion

3.1 Design and synthesis of the lipophilic derivatives of CA

Polyphenols serve as a treasure trove of therapeutic potential, offering powerful remedies for a range of disorders. CA, a low

molecular weight polyphenol with diverse pharmacological activities, holds significant therapeutic potential.[31] Jung et al. reported a significant blood glucose lowering effect of CA in C57BL/KsJ-db/db mice by enhancing glucose uptake in adipocytes and stimulating insulin secretion.[52] In addition, studies have discussed the antioxidant, anti-inflammatory and anti-glycation potential of CA.[53,54] However, its poor lipophilicity and low bioavailability pose significant restrictions in its further translational aspects. An in vivo study performed by Wang et al. revealed that the bioavailability and intestinal absorption of CA was just 14.70% and 12.40% respectively. In addition, a study done with Caco-2 cell model concluded that CA itself has poor Caco-2 monolayer permeability.[55] The pharmacokinetics of CA suggest that the absorption of CA occurs with the help of colonic microflora in the intestine via hydrolysis. Subsequently, it is subjected to enzyme conjugation (methylation, sulphation, and glucuronidation), making it more hydrophilic and resulting in rapid excretion. Therefore, masking the free carboxylic group can avoid rapid metabolism, thereby improving the bioavailability.[56]

Hence, to increase the absorption and bioavailability, chemical modification of CA was necessary either through esterification or amidation. It was found that the caffeic acid phenethyl ester (CAPE), in the rat plasma, showed rapid decomposition and removal from blood circulation due to the presence of esterases.[57] In contrast, the amide bond was found to be more stable compared to the ester due to high hydrolytic activation energy, which prevents rapid hydrolysis by esterases in the plasma. According to the report by Yang et al. the stability of caffeic acid phenethyl amide (CAPA) in rat plasma at 25 °C and 37 °C demonstrated 118-fold and 77-fold improvement compared to its ester form.[58] In view of bioavailability, a report by Matthias et al. assessed the bioavailability of echinacea components, mainly alkylamides and hydrophilic CA conjugates. They evaluated the permeability of these compounds in Caco-2 monolayer model and compared it in a phase I clinical trial. Interestingly, the in vitro result suggested a reduced membrane permeability of hydrophilic CA conjugates, whereas alkylamides showed rapid diffusion through Caco-2 monolayers, highlighting enhanced bioavailability. Similarly, in the clinical study, they could not detect the hydrophilic CA components in the plasma at any time point. On the other side, lipophilic alkylamides were detected in the plasma as early as 20 minutes of administration, suggesting increased bioavailability associated with lipophilic groups.[59,60]

Thus, based on the above observations and structural insights, we hypothesized that lipophilization of CA could enhance its cell permeability and, consequently, its bioavailability, leading to a more effective therapeutic effect. A recent work by Liu et al. showed that EGCG palmitate, inhibited α-amylase and α-glucosidase, 4.5 and 52 times better than that of EGCG as such.[37] Similarly, lipophilization of chlorogenic acid was found to be a better inhibitor of carbohydrate hydrolase compared to the parent molecule.[34] Furthermore, our group has employed an alkyl ether modification on EGCG, which offers enhanced metabolic stability by resisting hydrolysis as compared to EGCG palmitate work discussed above. This structural feature maintain the biological activity of the parent compound highlighting its multifaceted antidiabetic potential through the inhibition of α-amylase and α-glucosidase, as well as its antioxidant and anti-inflammatory properties.[33] Herein, we chose amidation over esterification to tune the lipid solubility and enhance the inhibitory properties as they are resistant towards the cleavage by esterases.[61] The alkyl amide derivatives of CA were synthesized in a single step with moderate to high yield as outlined below (Scheme 1).

3.2 In vitro α-glucosidase and α-amylase inhibition

CAn lipophilic derivatives were analysed for their inhibitory activity towards α-glucosidase and α-amylase. The non-linear regression curves were used to calculate the IC_{50} values of the derivatives for both α-glucosidase and α-amylase inhibitory activity (Table 1, Fig. S29 and S30). The parent molecule, CA, exhibited an IC_{50} of 12 400 μM against α-glucosidase. However, the addition of a hydrophobic chain led to a significant reduction in the IC_{50} value, enhancing the potency of CAn derivatives by a factor of 241 to 6392. Our synthesized derivatives showed enhanced α-glucosidase inhibition with an IC_{50} in the range (1.94–51.46 μM) compared to the standard drug acarbose (IC_{50} of 219.70 μM), and CA (IC_{50} 12 400 μM). Of note, the IC_{50} value for CA is not physiologically relevant. Among the compounds tested, **CA14**, with a 14-carbon long chain length, was found to be the most effective in inhibiting α-glucosidase, showing an IC_{50} of 1.94 μM, which is 113 times more potent than acarbose and 6392 times more potent than the parent molecule, CA. A similar trend was reported by Gutierrez et al. where they studied the inhibitory effect of alkyl gallates on the enzymatic digestion of starch. Their results were evident that the intermediate chain length of alkyl gallate was preferred for its inhibitory activity[62] which in turn supports the finding by Kaur and Singh[63] that amylose–lipid complex formation was more efficient with myristic acid (C14) than with stearic acid (C18) during cooking. Our most potent α-glucosidase inhibitor, **CA14** stood out as the most effective α-amylase inhibitor as well with an IC_{50} of 26.97 μM,
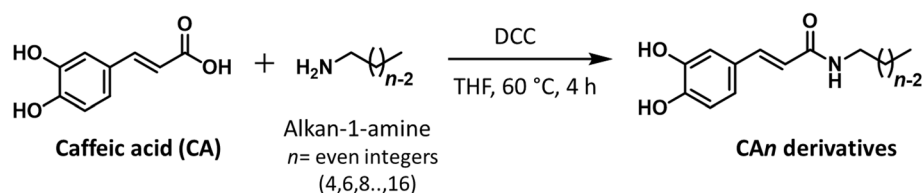
Scheme 1 Synthesis of lipophilic CAn derivatives via amide coupling, where n is an even number ranging from 4 to 16.

Table 1 Inhibitory potential of CA derivatives, acarbose, and Vitamin C against α-glucosidase, α-amylase, and DPPH radical. IC_{50} values are represented as mean ± SEM, with all experiments conducted in triplicate

Sl. no.	Compound	α-Glucosidase inhibition	α-Amylase inhibition	Antioxidant activity
		(IC_{50} ± SEM) in µM		
1	CA	12 400 ± 190	>500	34.27 ± 0.52
2	CA4	37.97 ± 1.57	>500	20.78 ± 0.45
3	CA6	51.46 ± 2.36	>500	23.74 ± 0.59
4	CA8	13.67 ± 0.44	>500	24.31 ± 0.58
5	CA10	19.13 ± 0.64	>500	23.37 ± 0.77
6	CA12	17.37 ± 0.87	72.83 ± 1.83	16.45 ± 0.48
7	**CA14**	**1.94 ± 0.06**	**26.97 ± 0.83**	**13.98 ± 0.38**
8	CA16	24.77 ± 0.46	58.42 ± 2.68	15.06 ± 0.30
9	Acarbose	219.70 ± 4.75	11.32 ± 0.23	No activity
10	Vitamin C	No activity	No activity	32.71 ± 0.47

closely resembling the inhibition potential of acarbose. The results suggest that the fourteen-carbon chain length of CA (**CA14**) strikes an optimal balance, offering sufficient length to fit into the active site without causing steric hindrance, while facilitating key interactions with the amino acids surrounding the active site. Taken together, **CA14**, emerged as the most potent compound, exhibiting multi-targeting properties. It inhibited α-glucosidase 113 times more effectively than acarbose and 6392 times better than CA, while also displaying α-amylase inhibition comparable to acarbose. Of note, the parent molecule showed no significant inhibitory activity against either enzyme. Further, to strengthen the *in vitro* study, we have conducted a co-inhibition study to assess the inhibitory potential of the compound **CA14** against α-glucosidase and α-amylase in the presence of each other. The results showed that the activity of individual enzymes remains largely unaffected by the presence of the other (Table S3).

3.3 Free radical scavenging capacity of CA*n* derivatives

Phenolic acids exhibit antioxidant activity that stems from their remarkable ability to neutralize reactive oxygen species (ROS), encompassing both radical and non-radical forms. As the antioxidant enzymes are limited in islet cells, the pancreatic β cells are highly susceptible to ROS-induced damage which in turn reduces insulin secretion. It can also react with DNA and proteins thereby complicating the condition of diabetes.[26,64] Studies have revealed that the presence of free hydroxyl groups, their number, and their position highly influence the antioxidant capability of polyphenolics compounds.[65,66] Recently, we have reported the excellent antioxidant properties of several EGCG derivatives.[32,33,67] Inspired by this, we explored whether lipophilic derivatives of CA could exhibit strong potential for reducing oxidative stress. The antioxidant potential of the synthesized CA derivatives were assessed using the DPPH assay where Vitamin C, a standard antioxidant was used as a reference (Table 1 and Fig. S31). The IC_{50} values obtained from non-linear regression curves ranged from 13.98–24.31 µM,

demonstrating their excellent antioxidant capacity compared to the standard Vitamin C (IC_{50} 32.71 µM). Of note, acarbose did not show any antioxidant activity. Among all the derivatives, **CA14**, the most potent compound with a 14-carbon chain length, was found to exhibit antioxidant activity 2.3 times more effectively than Vitamin C and 2.5 times better than CA. We have also chosen the previously reported potent EGCG-quinoxaline derivative, **15c**, and compared its antioxidant potential with that of **CA14**. Upon comparison, the antioxidant potentials of our synthesized derivatives, **CA14** (IC_{50} = 13.98 µM) and **15c** (IC_{50} = 16.83 µM) exhibited 2.3-fold and 2.0-fold better than the standard Vitamin C (IC_{50} = 32.71 µM). Further, among the lead compounds, **15c** and **CA14**, the antioxidant activity of **CA14** was found to be 1.2-fold better than that of **15c** (Fig. 1C). Overall, **CA14** exhibited multimodal behaviour by demonstrating superior α-glucosidase inhibition, comparable α-amylase inhibition, and enhanced antioxidant property, highlighting its potential as a multi-targeting antidiabetic agent (Fig. 1A–C).

3.4 Kinetic study of enzymatic inhibition by CA14

The synthesized CA derivatives demonstrated strong potency in inhibiting α-glucosidase, prompting us to conduct a detailed enzyme kinetics study to uncover the underlying inhibition mechanism. We took the most potent inhibitor (**CA14**) of α-glucosidase for the study keeping the acarbose as a reference. In a competitive inhibition, the inhibitor and the substrate will compete for the active site of the enzyme, which causes the maximum reaction velocity (V_{max}) unaltered and an increase in the Michaelis–Menten constant (K_m). The Lineweaver–Burk plot ($1/V$ *vs.* $1/S$), which was used to analyze the kinetics of α-glucosidase inhibition, shows that both acarbose and **CA14** were inhibited competitively (Fig. 2A and B). The V_{max} values for α-glucosidase inhibition by acarbose and **CA14** were 0.022 and 0.020 mM min^{-1}, respectively. The K_m and the inhibition constant (K_i) for acarbose were found as 0.681 mM and 395.5 µM, respectively. In comparison, **CA14** was found to exhibit a K_m value of 0.579 mM and a K_i value of 2.84 µM. Notably, the K_i value of **CA14** was about 140 times lower than that of acarbose, further supporting our findings that **CA14** had a significantly higher affinity for the enzyme, leading to superior inhibitory potential (Fig. 1C).

3.5 Inhibitory effects of CA14 on the formation of advanced glycation end products

Persistent hyperglycaemia results in the acceleration of non-enzymatic glycation reaction in the body, leading to the formation of AGEs. These molecules act as pro-inflammatory agents and trigger free radical production, further complicating diabetes.[68] We evaluated the inhibition of nonenzymatic glycosylation by **CA14** using model BSA-fructose glycosylation system. This process produces fructosamine and AGEs, which represent the early and late stages of glycosylation, respectively where the fluorescence intensity of AGEs serves as a key indicator of nonenzymatic glycosylation.[69,70] As displayed in Fig. 3A, on average, the standard antiglycation agent, AG which served
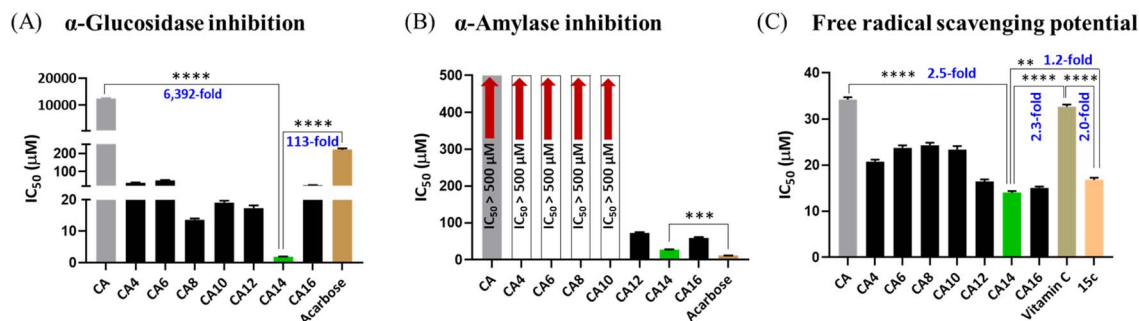
Fig. 1 Inhibitory effects of CA*n* derivatives against (A) α-glucosidase, (B) α-amylase, and (C) free radical scavenging potential, with acarbose serving as a reference inhibitor for enzymatic assays, while Vitamin C and **15c** as a reference for antioxidant potential, as acarbose lacked any antioxidant activity. One-way analysis of variance (ANOVA), with Dunnett's multiple comparison test, was used to determine the statistical significance of the data, where ** is represented for $p < 0.01$, *** for $p < 0.001$, and **** for $p < 0.0001$.
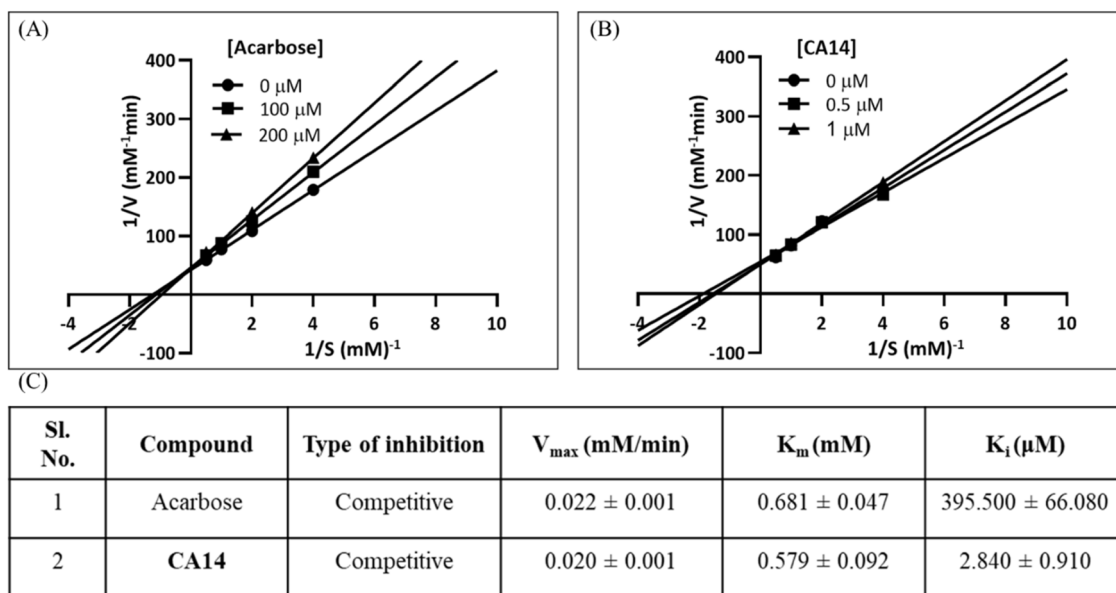

Sl. No.	Compound	Type of inhibition	V_{max} (mM/min)	K_m (mM)	K_i (μM)
1	Acarbose	Competitive	0.022 ± 0.001	0.681 ± 0.047	395.500 ± 66.080
2	**CA14**	Competitive	0.020 ± 0.001	0.579 ± 0.092	2.840 ± 0.910

Fig. 2 Lineweaver–Burk plots ($1/V$ *vs.* $1/S$) for α-glucosidase inhibition by (A) acarbose, (B) **CA14**, using α-pNPG as the substrate, and (C) calculated V_{max}, K_m, and K_i values illustrating the inhibitory properties of acarbose and **CA14**.

as a reference, was able to prevent the formation of fructosamine, an early stage glycation product, by 9% and 30% at 5 mM and 10 mM, respectively. On the other hand, our most potent compound, **CA14** showed an inhibition percentage of 33% and 70% at 5 mM and 10 mM respectively. The results reveal that **CA14** has an antiglycation potential several fold better than that of standard AG. The end stage glycation products, AGEs are highly reactive and have a significant contribution to complicate the condition of diabetes.[71] Hence, inhibiting the formation of AGEs may help prevent a cascade of pathological events. **CA14** demonstrated comparable inhibition of AGEs to that of AG (Fig. 3B). At 5 mM, **CA14** and AG exhibited 44% and 43% inhibition, respectively, while at 10 mM, the inhibition increased to 79% for **CA14** and 70% for AG. Moreover, the interaction of **CA14** with proteins prevented the proteins from reacting with fructose, thereby enhancing its antiglycation activity.

3.6 Binding affinity analysis and intrinsic fluorescence quenching of α-glucosidase and α-amylase in presence of CA14

Fluorescence spectroscopy serves as a reliable technique for assessing both the binding affinity and quenching potential of a ligand interacting with an enzyme. The intrinsic fluorescence of the proteins primarily arises from the tryptophan, tyrosine and phenylalanine residues. Among them, the indole group present in the tryptophan is highly sensitive towards the changes in the microenvironment making it suitable for the study accompanying the conformational changes in the proteins and their interactions with other molecules.[72,73] By observing the changes in the fluorescence emission peaks when excited at 280 nm with increasing ligand concentrations, one can learn more about the tryptophan and tyrosine residues and, consequently, the protein characteristics. Hence, we were interested in evaluating the intrinsic fluorescence quenching
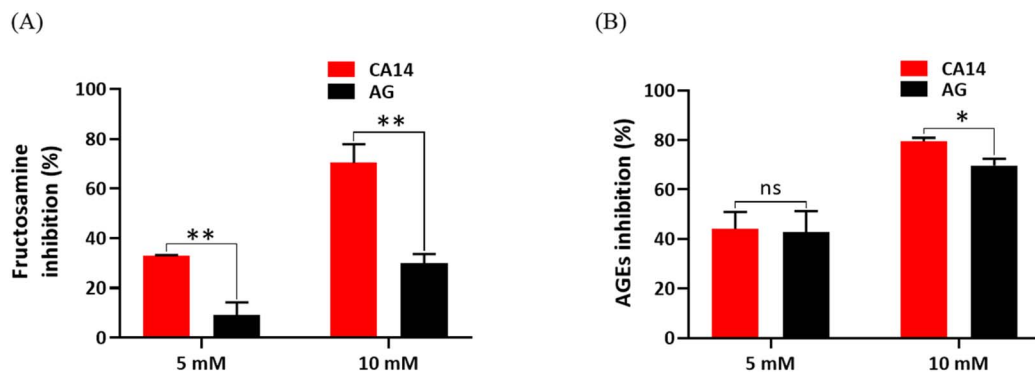
Fig. 3 Inhibitory effect of **CA14** and AG on the formation of (A) fructosamine and (B) AGEs in the BSA-fructose model. Student's *t*-test was used to determine the statistical significance of the data, where 'ns' represents not significant and is given for $p > 0.05$, * for $p < 0.05$, and ** for $p < 0.01$.

ability and binding affinity of the lead compound, **CA14**, with α-glucosidase and α-amylase at varying concentrations. With increasing concentration of **CA14**, we observed a decrease in the fluorescence intensity of both α-glucosidase and α-amylase (Fig. 4A and D). The findings imply that their interaction had altered the microenvironment surrounding the chromophore, resulting in fluorescence quenching. Stern–Volmer plots (Fig. 4B and E) were used to determine the Stern–Volmer quenching constant (K_{SV}) and the bimolecular quenching rate constant (K_q), while Scatchard plots (Fig. 4C and F) were employed to calculate the
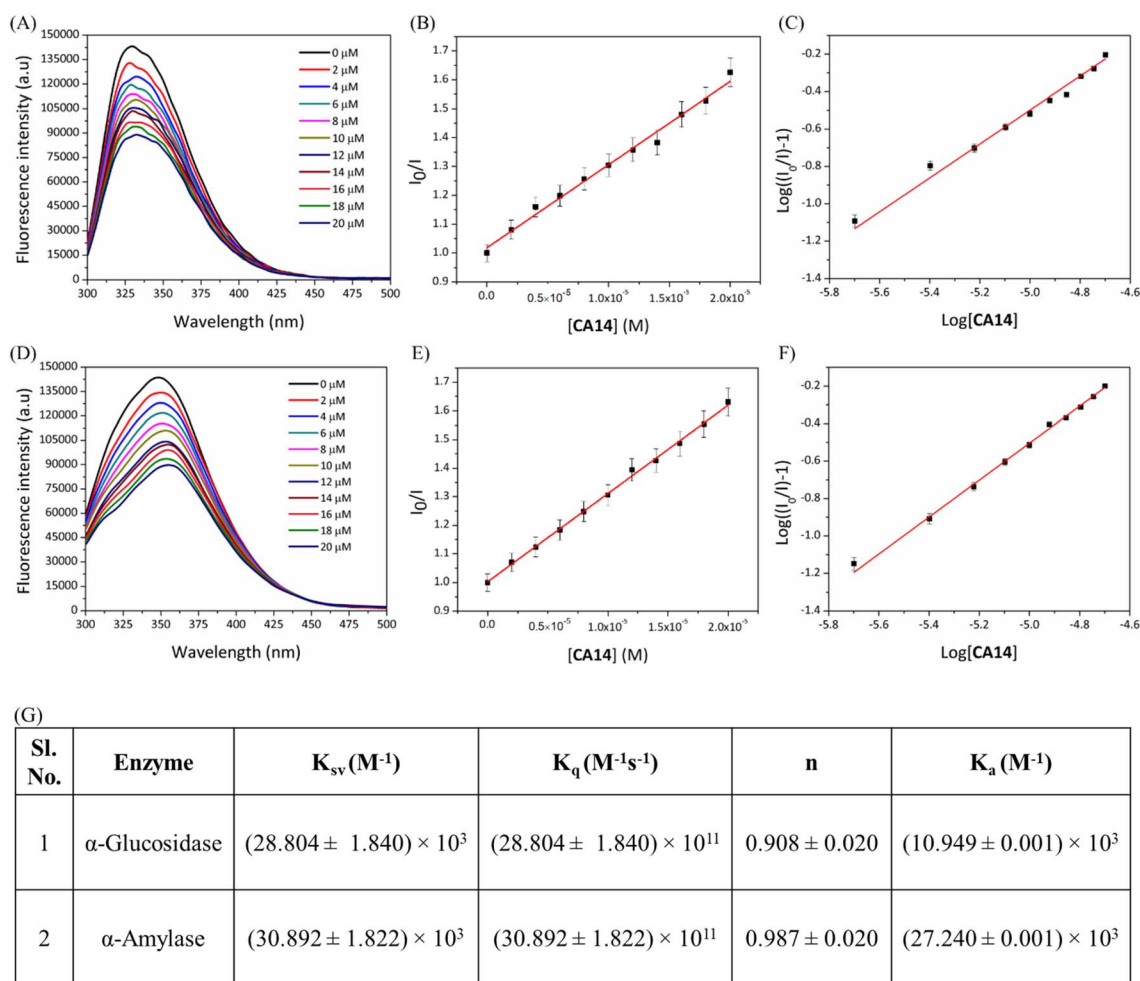

Sl. No.	Enzyme	K_{sv} (M^{-1})	K_q (M^{-1}s^{-1})	n	K_a (M^{-1})
1	α-Glucosidase	$(28.804 \pm 1.840) \times 10^3$	$(28.804 \pm 1.840) \times 10^{11}$	0.908 ± 0.020	$(10.949 \pm 0.001) \times 10^3$
2	α-Amylase	$(30.892 \pm 1.822) \times 10^3$	$(30.892 \pm 1.822) \times 10^{11}$	0.987 ± 0.020	$(27.240 \pm 0.001) \times 10^3$

Fig. 4 (A) Intrinsic fluorescence quenching of α-glucosidase in presence of **CA14** (0–20 μM); (B) and (C) corresponding Stern–Volmer plot and Scatchard plot, respectively; (D) intrinsic fluorescence quenching of α-amylase in the presence of **CA14** (0–20 μM); (E) and (F) corresponding Stern–Volmer plot and Scatchard plot, respectively; (G) calculated K_{SV}, K_q, n, and K_a values derived from Stern–Volmer and Scatchard plots.
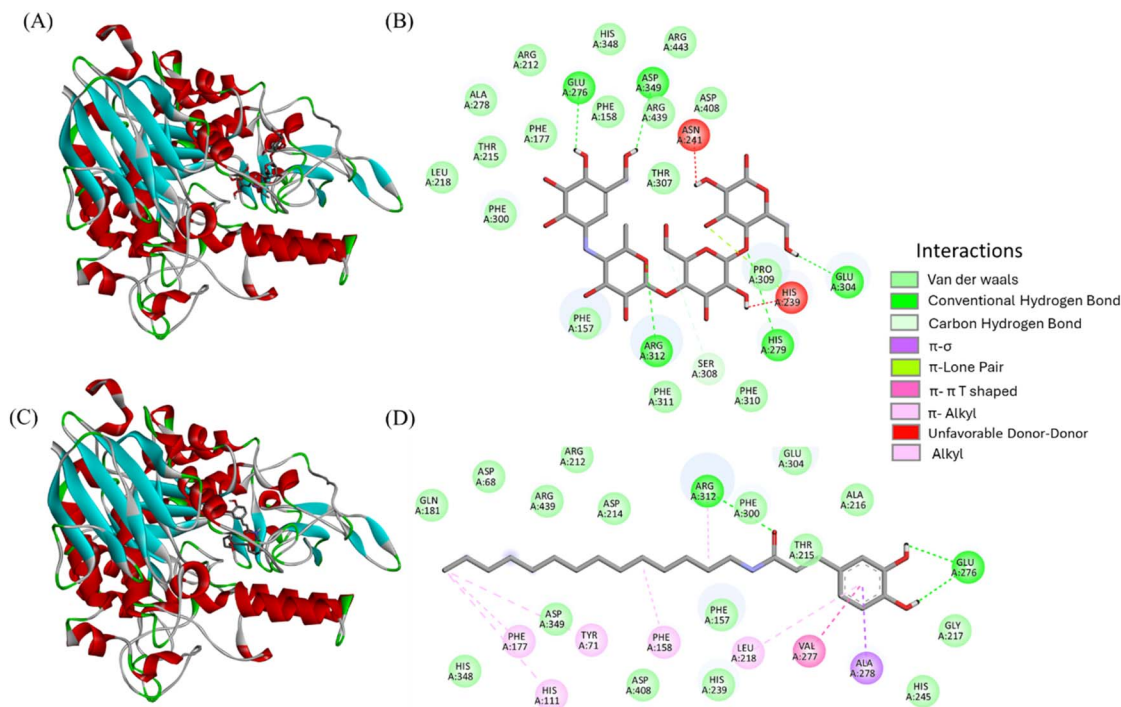
Fig. 5 Three-dimensional and two-dimensional molecular docking interaction profiles of (A and B) acarbose and (C and D) **CA14** within the active site of α-glucosidase.

binding constant (K_a) and the number of binding sites (n). K_{sv}, K_q, K_a, and n values for the interaction between **CA14** and α-glucosidase were 28.804×10^3 M^{-1}, 28.804×10^{11} M^{-1} s^{-1}, 10.949×10^3 M^{-1}, and 0.908 respectively. Similarly, for α-amylase, the corresponding values were found to be 30.892×10^3 M^{-1}, 30.892×10^{11} M^{-1} s^{-1}, 27.240×10^3 M^{-1}, and 0.987 respectively (Fig. 4G). The binding site value for both enzymes suggests the presence of at least one binding site for **CA14**, reinforcing its strong interaction. These findings indicate that **CA14** had strong affinities for both enzymes, leading to changes in the microenvironment of chromophores, as evidenced by its quenching behaviour.

3.7 *In silico* binding interactions of α-glucosidase and α-amylase with CA14

To get additional support for our experimental results, we performed molecular docking with **CA14** to understand its binding interactions with α-glucosidase and α-amylase. We used Auto-Dock Vina program to evaluate the docked conformations of **CA14** in the enzymes. α-Glucosidase contains the catalytic residues D214, E276, and D349 in its active site, while α-amylase has the key amino acid residues D197, E233, and D300 contributing to its active site. The docking analysis revealed that **CA14** interacted with the active site of α-glucosidase in a manner similar to acarbose, further supporting that the inhibition is competitive in nature. The *in silico* analysis for acarbose and **CA14** with α-glucosidase showed that the molecules occupied and interacted with the active site amino acid residues (Fig. 5A–D). With E276 and D349 residues, acarbose

demonstrated hydrogen bonding and Van der Waals interaction, respectively, while D214 showed no interaction (Fig. 5B). Interestingly, our most potent compound showed Van der Waals interaction with D214 and D349 while exhibiting hydrogen bonding with E276 residue (Fig. 5D). Moreover, **CA14** exhibited a strong binding affinity of −7.7 kcal mol^{-1} and −7.5 kcal mol^{-1} for acarbose, which further reveals a strong interaction with the enzyme (Table 2). The interactions of the compound within the active site of α-glucosidase were primarily driven by Van der Waals and hydrogen bonding. However, the compound was also surrounded by additional key amino acid residues as shown in Fig. 5D. The findings indicate that hydrogen bonding and hydrophobic interactions are the key forces involved between the enzyme and **CA14**. Further, the interaction of **CA14** with the Y71 and F300 has appeared to alter the microenvironment around this residue, leading to increased exposure to the solvent and a decrease in the fluorescence intensity. We believe that these interactions further reinforce our fluorescence quenching observations.

The binding affinity value of **CA14** (−6.8 kcal mol^{-1}) with α-amylase (Table 3) indicate that it also had a strong interaction. The *in silico* analysis for acarbose and **CA14** with α-amylase showed that the molecules occupied and interacted with the active site amino acid residues (Fig. 6A–D). The binding of **CA14** to the catalytic amino acid residues was predominantly governed by Van der Waals forces and hydrogen bonding. While acarbose showed no interaction with D197, it demonstrated hydrogen bonding with E233 and D300 residues (Fig. 6B). In contrast, our most potent compound, **CA14**, exhibited hydrogen bonding with D197 and Van der Waals interaction with both

     © 2025 The Author(s). Published by the Royal Society of Chemistry

Table 2 Binding affinity values (kcal mol⁻¹) and molecular interactions with the active site amino acid residues of α-glucosidase with acarbose and CA14

Sl. no.	Ligand of interest	Binding affinity (kcal mol⁻¹)	Active site amino acid residues		
			D214	E276	D349
1	Acarbose	−7.5	—	Hydrogen bond	Van der Waals
2	CA14	−7.7	Van der Waals	Hydrogen bond	Van der Waals

Table 3 Binding affinity values (kcal mol⁻¹) and molecular interactions with the active site amino acid residues in α-amylase by acarbose and CA14

Sl. no.	Ligand of interest	Binding affinity (kcal mol⁻¹)	Active site amino acid residues		
			D197	E233	D300
1	Acarbose	−7.8	—	Hydrogen bond	Hydrogen bond
2	CA14	−6.8	Hydrogen bond	Van der Waals	Van der Waals

E233 and D300 (Fig. 6D). It is interesting to note the presence of additional amino acid residues, including W58, W59, and Y62 of α-amylase (Fig. 6D) surrounding the compound, which aligned well with the fluorescence quenching study, further supporting the compound's interaction with α-amylase.

3.8 Effect of CA14 on the native conformation of enzymes using FT-IR spectroscopy

The structural changes in the α-glucosidase and α-amylase upon interaction with CA14 were explored using FT-IR. It has been reported that the proteins mainly show the existence of two characteristic amide bond peaks in the IR spectrum. It includes amide I (1700–1600 cm⁻¹) and amide II (1600–1500 cm⁻¹) regions characterized by the C=O and C–N stretching coupled with N–H bending respectively.[74] Nevertheless, the amide I band is highly sensitive and serves as a crucial indicator of the changes in the native conformations of the enzyme compared to the other bands.[75] In this study, the changes in the amide I region upon interaction between the enzyme and the ligand are predicted. As depicted in Fig. 7, the amide I peak for free α-glucosidase was observed at 1614.79 cm⁻¹ and for free α-amylase, the peak was at 1634.65 cm⁻¹ (Fig. S32). The peak near 3384.10 cm⁻¹ in Fig. 7 and at 3284.83 cm⁻¹ in Fig. S32 corresponds to the O–H stretching vibration. The interaction between the enzyme and CA14 exhibited spectral shifts without the emergence of any additional peaks, which indicate that the binding was driven by non-covalent interactions between them. Upon addition of CA14, we observed a significant red shift (Fig. 7) from (3384.10–3295.76 cm⁻¹), which indicates the presence of hydrogen bonding in the α-glucosidase–CA14 complex. As depicted in Fig. 7, the addition of CA14 had a pronounced blue shift in the amide I peak position from 1614.79 cm⁻¹ to 1633.46 cm⁻¹. Nevertheless, the addition of CA14 did not alter the amide I peak position in α-amylase, suggesting that the enzyme's chemical groups remained unchanged in the tested

concentration (Fig. S32). These findings demonstrate that in comparison to α-amylase, CA14 highly influenced the secondary structure of α-glucosidase by the rearrangement of the hydrogen bonding within the polypeptide groups.

3.9 Cytotoxicity assessment of CA14 in 3T3-L1 cell line

We aimed to assess the toxicity of CA14, in a non-malignant 3T3-L1 mammalian cell line, which has been widely used for investigating the cellular mechanisms associated with diabetes. We used MTT assay to assess the toxicity behaviour in mammalian cell lines. Viable or metabolically active cells reduce yellow tetrazolium salt to insoluble purple formazan crystals through the action of NAD(P)H-dependent oxidoreductase enzymes. The cell viability data (Fig. 8) revealed that CA14 exhibited no significant cytotoxicity up to 50 μM. Notably, the IC₅₀ values for α-glucosidase, α-amylase inhibition, and free radical quenching are below its cytotoxic dose, highlighting its potential as an effective and safe multimodal antidiabetic agent.

3.10 *In silico* physicochemical properties and ADMET studies

The drug-likeness assessed using Lipinski's rule of five (Ro5), helps to determine a molecule's bioavailability and general potential for drug development. The rule suggests that a drug candidate should have a molecular weight less than 500 Da, a threshold lipophilicity range (consensus log P ≤ 5), no more than 5 hydrogen bond donors, and no more than 10 hydrogen bond acceptors. Also, another criterion is to have topological polar surface area (TPSA) less than 140 Å².[76] Nevertheless, strict compliance to the Ro5 has hindered the development of novel therapeutic agents, including natural products, cyclic peptides, and macrocycles. Hence, the idea of beyond the rule of five (bRo5) was introduced to overcome the limitations of limitations of Ro5.[77] The bRo5 for a drug candidate includes the characteristics such as molecular weight greater than 700 Da,
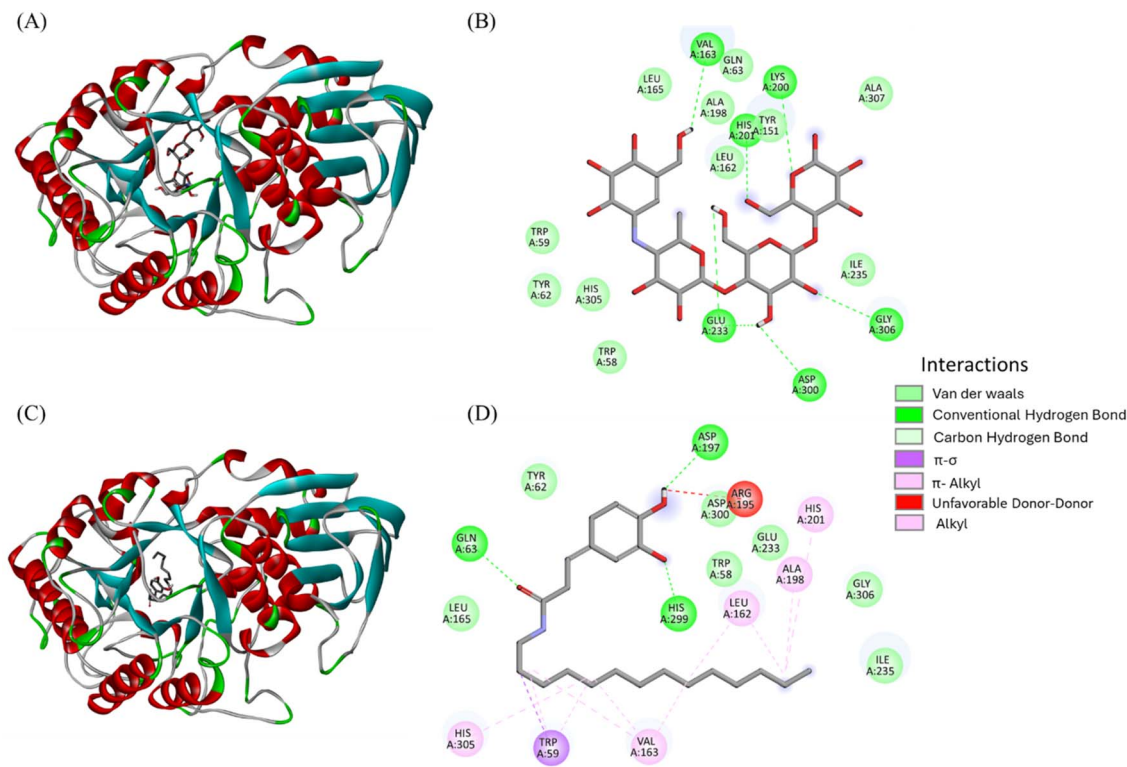
Fig. 6 Three-dimensional and two-dimensional molecular docking interaction profiles of (A and B) acarbose and (C and D) CA14 within the active site of α-amylase.

polar surface area (PSA) greater than 200 Å^2, no more than 5 hydrogen bond donors, and no more than 10 hydrogen bond acceptors, consensus log P < 0 or > 7.5, and number of rotatable bonds greater than 20. The physicochemical properties of CA14 (MW = 375.54 g mol^{-1}), along with 3 hydrogen bond donors and 3 hydrogen bond acceptors, showed a consensus log P value of 5.53, thus reflecting a balance between polarity and hydrophobicity of the molecule. Altogether, the compound complies with Lipinski's rule of five, with only one violation, while satisfying bRo5, showing its potential for an effective drug candidate. In addition, the TPSA for CA14 was found to be 69.56 Å^2, thereby showing the ability of the compound to penetrate the biological membrane due to low polar groups on the surface. Overall data of physicochemical characteristics has been represented in Table S1.

ADMET studies encompass properties such as human intestinal absorption, blood–brain barrier permeability (BBB), lethal dosage (LD$_{50}$) etc.[50] It is known that the primary site for a drug to get absorbed is the small intestine, and the data suggest that an absorption rate of less than 30% indicates poor druggability. CA14 exhibited a high percentage of human intestinal absorption (87.30%), which aligns with the criteria for potent drug-like molecules. The ability of a drug candidate to cross the BBB was measured as the logarithmic ratio of brain to plasma drug concentration (log BB). A value of log BB < −1 is considered to have low distribution in the brain, whereas a value greater than 3 shows high BBB penetration.[78] A value of −1.01 for BBB penetration further supports the limited

potential of CA14 to intrude the BBB, hence fewer side effects. Another parameter is the volume of distribution steady state (VDss). In contrast to drugs that bind to plasma proteins, which usually have a lower apparent volume of distribution, drugs that bind to tissues usually have a larger apparent volume of distribution. VDss is considered low if the value is less than −0.15 and is expressed in log L kg^{-1}.[79] The data revealed
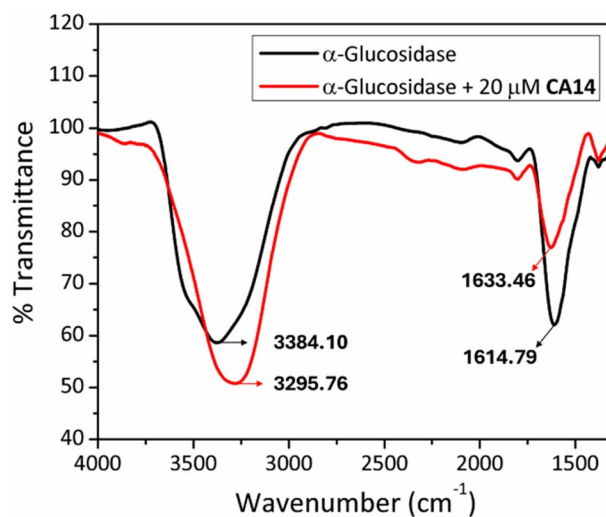

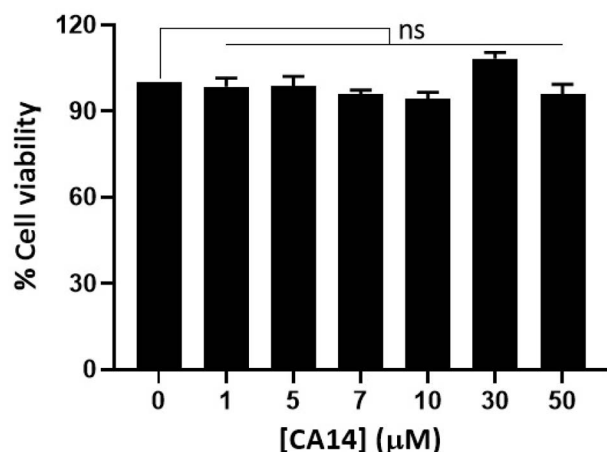Fig. 7 FT-IR spectra of α-glucosidase (7 μM) with and without CA14 (20 μM).

Fig. 8   3T3-L1 cell viability in the presence of varying concentration of CA14 (0–50 μM). One-way analysis of variance (ANOVA), with Dunnett's multiple comparison test, was used to determine the statistical significance of the difference in mean values. The statistical significance 'ns' represents not significant and is given for $p > 0.05$.

a greater apparent volume of distribution, with a value of 0.18, indicating the potential for **CA14** to be distributed more extensively in tissues rather than in plasma. LD_{50} is used as a measurement for toxicity prediction, representing the amount of the compound that causes the death of 50% group of the test animals. A value of $LD_{50} > 500$ mg kg^{-1} for a drug candidate is predicted to have low toxicity. The oral rat acute toxicity of **CA14** gave an LD_{50} of 2.37 mol kg^{-1}, indicating low toxicity. AMES toxicity is another test to assess the mutagenic property of a molecule, where a positive test suggests the potential of a compound to be carcinogenic in nature.[80] Interestingly, the compound was not found to have any AMES toxicity, suggesting it has a non-carcinogenic property (Table S2). Altogether, the compound has good pharmacokinetic properties and is safe to be considered to advance its therapeutic potential.

3.11   Stability assessment of CA14 under physiological conditions

We performed the stability assay to find the chemical stability of **CA14** under physiological conditions. After 10 days of incubation in 1X PBS of pH 7.4 at 37 °C, the **CA14**, extracted in the organic layer showed a single peak corresponding to the mass of **CA14** in the LC-MS (Fig. S33–S36). Notably, **CA14** did not exhibit any degradation even after incubating it for 10 days under physiological conditions, attesting to its stability.

4.   Conclusions

Diabetes, being a multifactorial disease, often renders treatment with a single therapeutic agent ineffective. To overcome these challenges, the development of antidiabetic agents with multimodal treatment strategies is essential. In this study, we developed a library of lipophilic derivatives of the small molecular weight polyphenol, caffeic acid (CA) in pursuit of potent multi-targeting antidiabetic molecules capable of inhibiting α-amylase and α-glucosidase, scavenging free radicals, and preventing the formation of AGEs. Among the synthesized compounds, **CA14** emerged as the most potent compound that inhibited α-glucosidase with an IC_{50} of 1.94 μM which is 113 times better than acarbose (IC_{50} of 219.70 μM) and 6392 times better than CA (IC_{50} of 12 400 μM). Additionally, **CA14** showed α-amylase inhibition comparable (IC_{50} of 26.97 μM) to that of acarbose (IC_{50} of 11.32 μM). An added advantage is its inhibitory effect against non-enzymatic glycation products, showing approximately 33% and 70% inhibition of early-stage fructosamine formation at 5 mM and 10 mM, respectively. This is significantly higher than AG, a known glycation inhibitor, which showed only 9% and 30% inhibition at the same concentrations. **CA14** also exhibited comparable inhibition of AGEs as that of AG. Further, it displayed superior free radical scavenging properties compared to standard Vitamin C, whereas the acarbose did not show any antioxidant activity. Kinetic study revealed that **CA14** inhibited the α-glucosidase competitively as that of acarbose. The intrinsic fluorescence quenching experiment revealed a significant interaction between **CA14** and both α-glucosidase and α-amylase which was further supported by molecular docking studies that demonstrated favorable binding interactions and affinities comparable to acarbose. The interactions between α-glucosidase and **CA14** were further analysed using FT-IR. Additionally, the compound did not exhibit any significant cytotoxicity in 3T3-L1 fibroblasts, even at 50 μM. Further, the ADMET profiling of **CA14** revealed good pharmacokinetic properties and is safe to be considered to advance its therapeutic potential. In addition, the **CA14** was found to be stable under physiological conditions. These findings highlight the critical role of strategic structural modifications in transforming natural products into advanced multimodal therapeutics, offering a promising avenue for tackling the intricate pathophysiology of diabetes.

Author contributions

S. S. conceived the idea and supervised the project; K. K. synthesized all the molecules, performed the enzymatic assays, antiglycation studies, enzyme kinetics, fluorescence studies, docking studies, ADMET studies, stability assay, and cell viability. S. S. and K. K. analysed the data.

Conflicts of interest

The authors of this work declare no conflict of interest.

Data availability

HPLC chromatogram, mass spectra, ^{1}H NMR, ^{13}C NMR, IC_{50} assessment against α-glucosidase, α-amylase, and free radicals for CA*n* derivatives has been provided in the supplementary information file. It also includes FT-IR spectra of α-amylase in presence of **CA14**, physicochemical properties and ADMET profiling, stability analysis, and co-inhibition study of α-glucosidase and α-amylase by **CA14**. See DOI: **https://doi.org/10.1039/d5ra05522a**.

Acknowledgements

References

1 L. Copeland, J. Blazek, H. Salman and M. C. Tang, Form and functionality of starch, *Food Hydrocolloids*, 2009, **23**, 1527–1534.

2 F. J. Warren, B. Zhang, G. Waltzer, M. J. Gidley and S. Dhital, The interplay of α-amylase and amyloglucosidase activities on the digestion of starch in *in vitro* enzymic systems, *Carbohydr. Polym.*, 2015, **117**, 192–200.

3 S. Hameed, Kanwal, F. Seraj, R. Rafique, S. Chigurupati, A. Wadood, A. U. Rehman, V. Venugopal, U. Salar, M. Taha and K. M. Khan, Synthesis of benzotriazoles derivatives and their dual potential as α-amylase and α-glucosidase inhibitors *in vitro*: Structure–activity relationship, molecular docking, and kinetic studies, *Eur. J. Med. Chem.*, 2019, **183**, 111677.

4 Y. X. Xu, Y. Y. Huang, R. R. Song, Y. L. Ren, X. Chen, C. Zhang, F. Mao, X. K. Li, J. Zhu, S. S. Ni, J. Wan and J. Li, Development of disulfide-derived fructose-1,6-bisphosphatase (FBPase) covalent inhibitors for the treatment of type 2 diabetes, *Eur. J. Med. Chem.*, 2020, **203**, 112500.

5 A. N. Kawde, M. Taha, R. S. Alansari, N. B. Almandil, E. H. Anouar, N. Uddin, F. Rahim, S. Chigurupati, M. Nawaz, S. Hayat, M. Ibrahim, P. K. Elakurthy, V. Vijayan, M. Morsy, H. Ibrahim, N. Baig and K. M. Khan, Exploring efficacy of indole-based dual inhibitors for α-glucosidase and α-amylase enzymes: *In silico*, biochemical and kinetic studies, *Int. J. Biol. Macromol.*, 2020, **154**, 217–232.

6 International Diabetes Federation, *IDF Diabetes Atlas 11*, 2025.

7 M. E. Singer, K. A. Dorrance, M. M. Oxenreiter, K. R. Yan and K. L. Close, The type 2 diabetes "modern preventable pandemic" and replicable lessons from the COVID-19 crisis, *Prev. Med. Rep.*, 2022, **25**, 101636.

8 K. Loh, H. Deng, A. Fukushima, X. Cai, B. Boivin, S. Galic, C. Bruce, B. J. Shields, B. Skiba, L. M. Ooms, N. Stepto, B. Wu, C. A. Mitchell, N. K. Tonks, M. J. Watt, M. A. Febbraio, P. J. Crack, S. Andrikopoulos and T. Tiganis, Reactive oxygen species enhance insulin sensitivity, *Cell Metab.*, 2009, **10**, 260–272.

9 M. A. Anis and Y. N. Sreerama, Inhibition of protein glycoxidation and advanced glycation end-product formation by barnyard millet (*Echinochloa frumentacea*) phenolics, *Food Chem.*, 2020, **315**, 126265.

10 M. Yousof Ali, S. Jannat and M. Mizanur Rahman, Ginsenoside derivatives inhibit advanced glycation end-product formation and glucose–fructose mediated protein glycation *in vitro via* a specific structure–activity relationship, *Bioorg. Chem.*, 2021, **111**, 104844.

11 H. Sugihara, M. Nagao, T. Harada, Y. Nakajima, K. Tanimura-Inagaki, F. Okajima, H. Tamura, T. Inazawa, T. Otonari, M. Kawakami and S. Oikawa, Comparison of three α-glucosidase inhibitors for glycemic control and bodyweight reduction in Japanese patients with obese type 2 diabetes, *J. Diabetes Invest.*, 2014, **5**, 206–212.

12 M. Nawaz, M. Taha, F. Qureshi, N. Ullah, M. Selvaraj, S. Shahzad, S. Chigurupati, A. Waheed and F. A. Almutairi, Structural elucidation, molecular docking, α-amylase and α-glucosidase inhibition studies of 5-amino-nicotinic acid derivatives, *BMC Chem.*, 2020, **14**, 43.

13 S. Poovitha and M. Parani, *In vitro* and *in vivo* α-amylase and α-glucosidase inhibiting activities of the protein extracts from two varieties of bitter gourd (*Momordica charantia* L.), *BMC Complementary Altern. Med.*, 2016, **16**, 185.

14 K. Aoki, T. Muraoka, Y. Ito, Y. Togashi and Y. Terauchi, Comparison of adverse gastrointestinal effects of acarbose and miglitol in healthy men: A crossover study, *Intern. Med. J.*, 2010, **49**, 1085–1087.

15 L. Zhang, Q. Chen, L. Li, J. S. W. Kwong, P. Jia, P. Zhao, W. Wang, X. Zhou, M. Zhang and X. Sun, Alpha-glucosidase inhibitors and hepatotoxicity in type 2 diabetes: A systematic review and meta-analysis, *Sci. Rep.*, 2016, **6**, 32649.

16 L. Zhang, S. Hogan, J. Li, S. Sun, C. Canning, S. J. Zheng and K. Zhou, Grape skin extract inhibits mammalian intestinal α-glucosidase activity and suppresses postprandial glycemic response in streptozocin-treated mice, *Food Chem.*, 2011, **126**, 466–471.

17 M. Mehrabi, S. Esmaeili, M. Ezati, M. Abassi, H. Rasouli, D. Nazari, H. Adibi and R. Khodarahmi, Antioxidant and glycohydrolase inhibitory behavior of curcumin-based compounds: Synthesis and evaluation of anti-diabetic properties *in vitro*, *Bioorg. Chem.*, 2021, **110**, 104720.

18 M. He, Y. Zhai, Y. Zhang, S. Xu, S. Yu, Y. Wei, H. Xiao and Y. Song, Inhibition of α-glucosidase by trilobatin and its mechanism: kinetics, interaction mechanism and molecular docking, *Food Funct.*, 2022, **13**, 857–866.

19 A. Kaur, B. Singh, B. Vyas and O. Silakari, Synthesis and biological activity of 4-aryl-3-benzoyl-5-phenylspiro[pyrrolidine-2.3′-indolin]-2′-one derivatives as novel potent inhibitors of advanced glycation end product, *Eur. J. Med. Chem.*, 2014, **79**, 282–289.

20 J. M. Ashraf, U. Shahab, S. Tabrez, E. J. Lee, I. Choi and S. Ahmad, Quercetin as a finer substitute to aminoguanidine in the inhibition of glycation products, *Int. J. Biol. Macromol.*, 2015, **77**, 188–192.

21 B. Niemann, S. Rohrbach, M. R. Miller, D. E. Newby, V. Fuster and J. C. Kovacic, Oxidative stress and cardiovascular risk: Obesity, diabetes, smoking, and

pollution: Part 3 of a 3-part series, *J. Am. Coll. Cardiol.*, 2017, **70**, 230–251.

22 F. Asgharpour Dil, Z. Ranjkesh and M. T. Goodarzi, A systematic review of antiglycation medicinal plants, *Diabetes Metab. Syndr.: Clin. Res. Rev.*, 2019, **13**, 1225–1229.

23 K. M. Khan, S. Saeed, M. Ali, M. Gohar, J. Zahid, A. Khan, S. Perveen and M. I. Choudhary, Unsymmetrically disubstituted urea derivatives: A potent class of antiglycating agents, *Bioorg. Med. Chem.*, 2009, **17**, 2447–2451.

24 A. Adamczak, M. Ożarowski and T. M. Karpiński, Curcumin, a natural antimicrobial agent with strain-specific activity, *Pharmaceuticals*, 2020, **13**, 153.

25 D. G. I. Kingston, G. Samranayake and C. A. Ivey, The chemistry of taxol, a clinically useful anticancer agent, *J. Nat. Prod.*, 1990, **53**, 1–12.

26 K. Kannan, J. A. George, R. Sahadevan, M. Kothari and S. Sadhukhan, Insights into one drug, multi-target aspects of polyphenols for diabetes management: *in vitro, in vivo*, and clinical evidence, *Phytochem. Rev.*, 2024, DOI: 10.1007/s11101-024-10047-9.

27 R. Sahadevan, A. Binoy, I. Shajan and S. Sadhukhan, Mitochondria-targeting EGCG derivatives protect H9c2 cardiomyocytes from H_2O_2-induced apoptosis: Design, synthesis and biological evaluation, *RSC Adv.*, 2023, **13**, 29477–29488.

28 M. Aijaz, N. Keserwani, M. Yusuf, N. H. Ansari, R. Ushal and P. Kalia, Chemical, biological, and pharmacological prospects of caffeic acid, *Biointerface Res. Appl. Chem.*, 2023, **13**, 324.

29 H. R. El-Seedi, A. M. A. El-Said, S. A. M. Khalifa, U. Göransson, L. Bohlin, A. K. Borg-Karlson and R. Verpoorte, Biosynthesis, natural sources, dietary intake, pharmacokinetic properties, and biological activities of hydroxycinnamic acids, *J. Agric. Food Chem.*, 2012, **60**, 10877–10895.

30 E. J. Iweala, O. E. Adurosakin, U. Innocent, C. A. Omonhinmin, O. E. Dania and E. A. Ugbogu, Anti-aging potential of bioactive phytoconstituents found in edible medicinal plants: A review, *Sci*, 2024, **6**, 36.

31 C. Manach, A. Scalbert, C. Morand, C. Rémésy and L. Jiménez, Polyphenols: Food sources and bioavailability, *Am. J. Clin. Nutr.*, 2004, **79**, 727–747.

32 M. Kothari, K. Kannan, R. Sahadevan and S. Sadhukhan, Novel molecular hybrids of EGCG and quinoxaline: Potent multi-targeting antidiabetic agents that inhibit α-glucosidase, α-amylase, and oxidative stress, *Int. J. Biol. Macromol.*, 2024, **263**, 130175.

33 M. Kothari, K. Kannan, R. Sahadevan, S. V. Retnakumar, C. Chauvin, J. Bayry and S. Sadhukhan, Lipophilic derivatives of EGCG as potent α-amylase and α-glucosidase inhibitors ameliorating oxidative stress and inflammation, *Bioorg. Chem.*, 2024, **153**, 107786.

34 S. Wang, Y. Li, D. Huang, S. Chen, Y. Xia and S. Zhu, The inhibitory mechanism of chlorogenic acid and its acylated derivatives on α-amylase and α-glucosidase, *Food Chem.*, 2022, **372**, 131334.

35 Y. Self-Medlin, J. Byun, R. F. Jacob, Y. Mizuno and R. P. Mason, Glucose promotes membrane cholesterol crystalline domain formation by lipid peroxidation, *Biochim. Biophys. Acta, Biomembr.*, 2009, **1788**, 1398–1403.

36 S. C. R. Sherratt, P. Villeneuve, E. Durand and R. P. Mason, Rosmarinic acid and its esters inhibit membrane cholesterol domain formation through an antioxidant mechanism based, in nonlinear fashion, on alkyl chain length, *Biochim. Biophys. Acta, Biomembr.*, 2019, **1861**, 550–555.

37 B. Liu, Z. Kang and W. Yan, Synthesis, stability, and antidiabetic activity evaluation of (−)-epigallocatechin gallate (EGCG) palmitate derived from natural tea polyphenols, *Molecules*, 2021, **26**, 393.

38 M. Ali, M. Hassan, S. A. Ansari, H. M. Alkahtani, L. S. Al-Rasheed and S. A. Ansari, Quercetin and kaempferol as multi-targeting antidiabetic agents against mouse model of chemically induced type 2 diabetes, *Pharmaceuticals*, 2024, **17**, 757.

39 V. P. Tassopoulou, A. Tzara and A. P. Kourounakis, Design of improved antidiabetic drugs: A journey from single to multitarget agents, *ChemMedChem*, 2022, **17**, e202200320.

40 Z. Liu, J. Fu, L. Shan, Q. Sun and W. Zhang, Synthesis, preliminary bioevaluation and computational analysis of caffeic acid analogues, *Int. J. Mol. Sci.*, 2014, **15**, 8808–8820.

41 H. X. Xu, H. Chen, Z. P. Yin and Q. F. Zhang, Piceid dicarboxylic acid esters as potent α-glucosidase inhibitors and antiglycation agents: Synthesis, spectroscopic and molecular docking studies, *J. Mol. Struct.*, 2024, **1296**, 136938.

42 Z. Han, L. Wang, P. Sun, M. Huang, F. Yu, J. Liu, Y. Wu, P. He, Y. Tu and B. Li, Quinic acid as an inhibitor of α-glucosidase activity, nonenzymatic glycosylation, and glucose transport in Caco-2 cells, *Food Front.*, 2024, **5**, 2545–2555.

43 S. Bienert, A. Waterhouse, T. A. P. De Beer, G. Tauriello, G. Studer, L. Bordoli and T. Schwede, The SWISS-MODEL repository-new features and functionality, *Nucleic Acids Res.*, 2017, **45**, D313–D319.

44 O. Trott and A. J. Olson, AutoDock Vina: Improving the speed and accuracy of docking with a new scoring function, efficient optimization, and multithreading, *J. Comput. Chem.*, 2010, **31**, 455–461.

45 S. Chauhan, M. Srivastava, and J. Singh, DocVSP (Docking-based Virtual Screening Perl-script) for automating and integrating AutoDock & SBDD, in *SCRS Conference Proceedings on Intelligent Systems*, 2021, pp. 287–291.

46 Y. Huang, S. J. Richardson, C. S. Brennan and S. Kasapis, Mechanistic insights into α-amylase inhibition, binding affinity and structural changes upon interaction with gallic acid, *Food Hydrocolloids*, 2024, **148**, 109467.

47 C. Gilles, J. P. Astier, G. Marchis-Mouren, C. Cambillau and F. Payan, Crystal structure of pig pancreatic α-amylase isoenzyme II, in complex with the carbohydrate inhibitor acarbose, *Eur. J. Biochem.*, 1996, **238**, 561–569.

48 Y. Zheng, J. Tian, W. Yang, S. Chen, D. Liu, H. Fang, H. Zhang and X. Ye, Inhibition mechanism of ferulic acid

against α-amylase and α-glucosidase, *Food Chem.*, 2020, **317**, 126346.

49 A. Daina, O. Michielin and V. Zoete, SwissADME: A free web tool to evaluate pharmacokinetics, drug-likeness and medicinal chemistry friendliness of small molecules, *Sci. Rep.*, 2017, **7**, 42717.

50 D. E. V Pires, T. L. Blundell and D. B. Ascher, pkCSM: Predicting small-molecule pharmacokinetic and toxicity properties using graph-based signatures, *J. Med. Chem.*, 2015, **58**, 4066–4072.

51 S. Singh, M. F. Sk, A. Sonawane, P. Kar and S. Sadhukhan, Plant-derived natural polyphenols as potential antiviral drugs against SARS-CoV-2 *via* RNA-dependent RNA Polymerase (RdRp) inhibition: An *in-silico* analysis, *J. Biomol. Struct. Dyn.*, 2021, **39**, 6249–6264.

52 U. J. Jung, M. K. Lee, Y. B. Park, S. M. Jeon and M. S. Choi, Antihyperglycemic and antioxidant properties of caffeic acid in db/db mice, *J. Pharmacol. Exp. Ther.*, 2006, **318**, 476–483.

53 X. Cao, Y. Xia, M. Zeng, W. Wang, Y. He and J. Liu, Caffeic acid inhibits the formation of advanced glycation end products (AGEs) and mitigates the AGEs-induced oxidative stress and inflammation reaction in human umbilical vein endothelial cells (HUVECs), *Chem. Biodiversity*, 2019, **16**, e1900174.

54 C. Chao, M. Mong, K. Chan and M. Yin, Anti-glycative and anti-inflammatory effects of caffeic acid and ellagic acid in kidney of diabetic mice, *Mol. Nutr. Food Res.*, 2010, **54**, 388–395.

55 S. J. Wang, J. Zeng, B. K. Yang and Y. M. Zhong, Bioavailability of caffeic acid in rats and its absorption properties in the Caco-2 cell model, *Pharm. Biol.*, 2014, **52**, 1150–1157.

56 M. Alam, G. M. Ashraf, K. Sheikh, A. Khan, S. Ali, M. M. Ansari, M. Adnan, V. R. Pasupuleti and M. I. Hassan, Potential therapeutic implications of caffeic acid in cancer signaling: Past, present, and future, *Front. Pharmacol.*, 2022, **13**, 1–14.

57 X. Wang, P. D. Bowman, S. M. Kerwin and S. Stavchansky, Stability of caffeic acid phenethyl ester and its fluorinated derivative in rat plasma, *Biomed. Chromatogr.*, 2007, **21**, 343–350.

58 J. Yang, S. M. Kerwin, P. D. Bowman and S. Stavchansky, Stability of caffeic acid phenethyl amide (CAPA) in rat plasma, *Biomed. Chromatogr.*, 2012, **26**, 594–598.

59 A. Matthias, J. T. Blanchfield, K. G. Penman, I. Toth, C. S. Lang, J. J. De Voss and R. P. Lehmann, Permeability studies of alkylamides and caffeic acid conjugates from echinacea using a Caco-2 cell monolayer model, *J. Clin. Pharm. Ther.*, 2004, **29**, 7–13.

60 A. Matthias, K. G. Penman, N. J. Matovic, K. M. Bone, J. J. De Voss and R. P. Lehmann, Bioavailability of echinacea constituents: Caco-2 monolayers and pharmacokinetics of the alkylamides and caffeic acid conjugates, *Molecules*, 2005, **10**, 1242–1251.

61 R. Sahadevan, S. Singh, A. Binoy and S. Sadhukhan, Chemico-biological aspects of (−)-epigallocatechin-3-gallate (EGCG) to improve its stability, bioavailability and membrane permeability: Current status and future prospects, *Crit. Rev. Food Sci. Nutr.*, 2023, **63**, 10382–10411.

62 A. S. A. Gutierrez, J. Guo, J. Feng, L. Tan and L. Kong, Inhibition of starch digestion by gallic acid and alkyl gallates, *Food Hydrocolloids*, 2020, **102**, 105603.

63 K. Kaur and N. Singh, Amylose-lipid complex formation during cooking of rice flour, *Food Chem.*, 2000, **71**, 511–517.

64 H. Kaneto, Y. Kajimoto, J. Miyagawa, T. Matsuoka, Y. Fujitani, Y. Umayahara, T. Hanafusa, Y. Matsuzawa, Y. Yamasaki and M. Hori, Beneficial effects of antioxidants in diabetes: Possible protection of pancreatic beta-cells against glucose toxicity, *Diabetes*, 1999, **48**, 2398–2406.

65 V. Srivastava, M. P. Darokar, A. Fatima, J. K. Kumar, C. Chowdhury, H. O. Saxena, G. R. Dwivedi, K. Shrivastava, V. Gupta, S. K. Chattopadhyay, S. Luqman, M. M. Gupta, A. S. Negi and S. P. S. Khanuja, Synthesis of diverse analogues of oenostacin and their antibacterial activities, *Bioorg. Med. Chem.*, 2007, **15**, 518–525.

66 Y. Sato, S. Itagaki, T. Kurokawa, J. Ogura, M. Kobayashi, T. Hirano, M. Sugawara and K. Iseki, *In vitro* and *in vivo* antioxidant properties of chlorogenic acid and caffeic acid, *Int. J. Pharm.*, 2011, **403**, 136–138.

67 S. Singh, R. Sahadevan, R. Roy, M. Biswas, P. Ghosh, P. Kar, A. Sonawane and S. Sadhukhan, Structure-based design and synthesis of a novel long-chain 4″-alkyl ether derivative of EGCG as potent EGFR inhibitor: *In vitro* and *in silico* studies, *RSC Adv.*, 2022, **12**, 17821–17836.

68 P. Meenatchi, A. Purushothaman and S. Maneemegalai, Antioxidant, antiglycation and insulinotrophic properties of *Coccinia grandis* (L.) *in vitro*: Possible role in prevention of diabetic complications, *J. Tradit. Complementary Med.*, 2017, **7**, 54–64.

69 L. Zeng, H. Ding, X. Hu, G. Zhang and D. Gong, Galangin inhibits α-glucosidase activity and formation of non-enzymatic glycation products, *Food Chem.*, 2019, **271**, 70–79.

70 M. Khalid, G. Petroianu and A. Adem, Advanced glycation end products and diabetes mellitus: Mechanisms and perspectives, *Biomolecules*, 2022, **12**, 542.

71 S. Awasthi and N. T. Saraswathi, Sinigrin, a major glucosinolate from cruciferous vegetables restrains non-enzymatic glycation of albumin, *Int. J. Biol. Macromol.*, 2016, **83**, 410–415.

72 Y. Chen and M. D. Barkley, Toward understanding tryptophan fluorescence in proteins, *Biochemistry*, 1998, **37**, 9976–9982.

73 I. Weinryb and R. F. Steiner, Luminescence of the tryptophan and tyrosine residues of papain in solution, *Biochemistry*, 1970, **9**, 135–146.

74 E. Goormaghtigh, V. Cabiaux and J. M. Ruysschaert, Secondary structure and dosage of soluble and membrane proteins by attenuated total reflection Fourier-transform infrared spectroscopy on hydrated films, *Eur. J. Biochem.*, 1990, **193**, 409–420.

75 G. Zandomeneghi, M. R. H. Krebs, M. G. McCammon and M. Fändrich, FTIR reveals structural differences between

native β-sheet proteins and amyloid fibrils, *Protein Sci.*, 2004, **13**, 3314–3321.

76 X. M. Liao, X. Y. Li, Y. Wang, H. Fu, L. Zhang, T. Z. Li and C. A. Geng, Synthesis of diarylpentane derivatives as novel α-glucosidase inhibitors: Their inhibitory mechanism and hypoglycemic effects, *Eur. J. Med. Chem.*, 2025, **300**, 118161.

77 D. H. O' Donovan, C. De Fusco, L. Kuhnke and A. Reichel, Trends in molecular properties, bioavailability, and permeability across the Bayer compound collection, *J. Med. Chem.*, 2023, **66**, 2347–2360.

78 J. D. Sánchez-Martínez, A. Valdés, R. Gallego, Z. J. Suárez-Montenegro, M. Alarcón, E. Ibañez, G. Alvarez-Rivera and A. Cifuentes, Blood–brain barrier permeability study of potential neuroprotective compounds recovered from plants and agri-food by-products, *Front. Nutr.*, 2022, **9**, 924596.

79 L. Guan, H. Yang, Y. Cai, L. Sun, P. Di, W. Li, G. Liu and Y. Tang, ADMET-score—A comprehensive scoring function for evaluation of chemical drug-likeness, *MedChemComm*, 2019, **10**, 148–157.

80 E. Zeiger, The test that changed the world: The AMES test and the regulation of chemicals, *Mutat. Res., Genet. Toxicol. Environ. Mutagen.*, 2019, **841**, 43–48.